Structure, energy, and electronic states of vacancies in Ge nanocrystals

Kenneth Bayus
Department of Material Science and Engineering, Cornell University, Ithaca, New York 14850, USA

Oscar Paz*
Department of Physics and Astronomy, Rutgers University, Piscataway, New Jersey 08854-8019, USA

S. P. Beckman†
Department of Material Science and Engineering, Iowa State University, Ames, Iowa 50014, USA

(Received 1 June 2010; published 6 October 2010)

The atomic structure, energy of formation, and electronic states of vacancies in H-passivated Ge nanocrystals are studied by density-functional theory methods. The competition between quantum self-purification and the free surface relaxations is investigated. The free surfaces of crystals smaller than 2 nm distort the Jahn-Teller relaxation and enhance the reconstruction bonds. This increases the energy splitting of the quantum states and reduces the energy of formation to as low as 1 eV per defect in the smallest nanocrystals. In crystals larger than 2 nm the observed symmetry of the Jahn-Teller distortion matches the symmetry expected for bulk Ge crystals. Near the nanocrystal's surface the vacancy is found to have an energy of formation no larger than 0.5–1.4 eV per defect, but a vacancy more than 0.7 nm inside the surface has an energy of formation that is the same as in bulk Ge. No evidence of the self-purification effect is observed; the dominant effect is the free surface relaxations, which allow for the enhanced reconstruction. From the evidence in this paper, it is predicted that for moderate sized Ge nanocrystals a vacancy inside the crystal will behave bulklike and not interact strongly with the surface, except when it is within 0.7 nm of the surface.

DOI: 10.1103/PhysRevB.82.155409 PACS number(s): 66.30.Pa, 73.22.−f, 61.46.−w, 61.72.uf

I. INTRODUCTION

Germanium is a particularly attractive material for use in semiconducting devices. The charge carriers have a high mobility due to their low effective mass and it is possible to achieve a high level of *n*- and *p*-type dopant activation.[1,2] The designers of microelectronics initially focused on Si instead of Ge because Ge lacks a native oxide that can be used as a dielectric. Fortunately this limitation can be overcome by several techniques that have been developed within the last decade: a thin Si overlayer can be grown over the Ge so that SiO_2 can be used as the dielectric,[3] a Ge-oxynitride dielectric layer can be grown over the Ge (Ref. 4) or a high-κ dielectric crystal, such as ZrO_2, can be used in the device.[5] These techniques allow for the development of Si/Ge heterostructure devices such as metal-oxide-semiconductor field effect transistors, MOSFETs. The heterostructure MOSFET is primarily Si so existing fabrication technology can be used, but Ge is included as a buried channel between the source and drain to allow for high-speed conductivity.[6–9]

Before Ge can become an industrially important material, it must be possible to introduce and control a variety of dopant species in the crystal.[10] Due to the initial challenge of finding a suitable dielectric material, there has been much less effort in understanding Ge as compared to Si. Subsequently much less is known about the control of dopants in Ge than in Si. There exists a close relationship between impurity diffusion and self-diffusion; therefore, it is fundamentally important to understand self-diffusion to understand the control of impurity atoms.

Following Refs. 11 and 12, the self-diffusion coefficient $D(T)$ is written as a sum of the vacancy (v), interstitial (i), and direct-exchange (ex) diffusion mechanisms,

$$D(T) = f_v(T)C_v^{eq}(T)D_v(T) + f_i(T)C_i^{eq}(T)D_i(T) + D_{ex}(T), \tag{1}$$

where $f_\eta(T)$ are correlation factors, $C_\eta^{eq}(T)$ are the equilibrium concentrations of the intrinsic defects, and $D_\eta(T)$ are the diffusion coefficients corresponding to $\eta = v, i, ex$. The concentrations and diffusion coefficients are expressed in terms of their thermodynamic quantities,

$$C_\eta^{eq}(T) = \exp\left[\frac{\Delta S_f^\eta}{k_B}\right]\exp\left[-\frac{\Delta E_f^\eta}{k_B T}\right], \tag{2}$$

$$D_\eta(T) = K_m \exp\left[\frac{\Delta S_m^\eta}{k_B}\right]\exp\left[-\frac{\Delta E_m^\eta}{k_B T}\right], \tag{3}$$

where ΔS_f^η and ΔE_f^η are the entropy and energy of formation, ΔS_m^η and ΔE_m^η are the entropy and energy of migration, k_B is the Boltzmann constant, and K_m is a constant prefactor. The constant K_m is independent of temperature and depends on the lattice geometry and the vibrational frequencies. The entropy terms include both the configurational and the vibrational entropies. The energy of formation is determined by the atomic bonding at the defect site and the energy of migration is determined by the energy of the saddle-point configuration along the minimum-energy transition path between stable atomic configurations.

Direct exchange is the slowest diffusion mechanism. Straining the lattice to allow the atoms to move past each other requires a prohibitively large amount of energy. The principal diffusion pathways involve either vacancy- or interstitial-assisted migration. The work presented here focuses on these intrinsic point defects. Based on the energies

TABLE I. The energies of formation and migration for vacancies and interstitial defects in Si and Ge (in eV).

Element	ΔE_f^v	ΔE_f^i	ΔE_m^v	ΔE_m^i
Si	3.1–3.6 (Ref. 13)	3.2 (Ref. 14)	0.4–1.40 (Ref. 13)	0.45 (Ref. 15)
	3.7 (Ref. 16)	3.31–3.84 (Ref. 17)	0.43–0.49 (Ref. 12)	0.84 (Ref. 12)
	3.49 (Ref. 18)	3.27 (Ref. 19)		
	3.53 (Ref. 20)			
Ge	2.3 (Ref. 21)	2.29 (Ref. 22)	0.7 (Ref. 23)	0.5 (Ref. 24)
	1.7–2.0 (Ref. 25)	2.3–4.1 (Ref. 26)	0.36–0.7 (Ref. 27)	
	2.4 (Ref. 23)	3.55 (Ref. 28)		
	2.6 (Ref. 27)	3.50 (Ref. 29)		
	2.56 (Ref. 29)			

listed in Table I the self-diffusion coefficient in Si is controlled by a self-interstitial kick-out mechanism at high temperatures ($T>900$ °C) and vacancy-mediated diffusion at lower temperatures.[13]

In Ge, vacancy-assisted diffusion is the primary mode.[30] Although the migration barrier for Ge vacancies and self-interstitials is roughly equivalent, the energy of formation for interstitial Ge atoms is approximately 1 eV greater than vacancies whereas in Si the energy to create vacancies and interstitials is equivalent. In Ge self-interstitial atoms will only be formed at very high temperatures or after highly energetic processes such as irradiation.[31] Therefore, vacancies in Ge are substantially more influential than interstitial atoms for assisting diffusion under thermal equilibrium, as compared to Si.

The dominance of vacancies-assisted diffusion is observed experimentally, both for self-diffusion[32] and impurity-atom diffusion.[30,33,34] The interaction between vacancies and impurity atoms is complicated. It is believed that vacancies and impurities form mobile defect pairs.[26,35,36] This defect pair can become pinned when a second impurity, such as C, joins the complex.[26] In addition to forming complexes, the vacancies and impurities often carry a charge.[21,26,35] It is likely that an isolated vacancy in bulk Ge is charged −2.[35] In the work presented here only isolated, charge neutral, impurities are investigated, which is consistent with the nanoscale context of this study.

To improve the engineering control of material properties and increase device efficiency, it is desirable to move from bulk to nanoscale structures. There are many examples of situations where nanostructured Ge offers benefits. The use of Ge nanocrystals as the floating gate of MOS memory devices results in a dramatic shift in the threshold-voltage, improved switching characteristics, and decreased leakage current.[37,38] Ge films with nanostructured surfaces offer the ability to tune the optical properties of thin films.[39] Ge nanowires are considered for use as MOSFETs.[40,41]

Ultimately the nanostructures used to create devices need to be tailored by controlling their size, surfaces, and dopants. With respect to introducing dopants, the electronic properties of nanostructures are believed to be sensitive to the relative position of the impurities in the structure. The mean free path of charge carriers within nanowires depends strongly on the radial dopant profile.[42] This will influence the conductivity. In addition to the challenge of selectively incorporating the dopant atoms into the nanostructure, the impurity distribution must be maintained for the lifetime of the device.

At the quantum scale the primary difference between a bulk crystal and a nanocrystal is the interaction of the wave function with the surfaces. As the size of a structure decreases, the crystal's translational symmetry ceases to be meaningful. The electronic band structure that is nominally a function of the quantum number $\mathbf{k}$ is projected onto the Γ point in the center of the Brillouin zone. The crystal's energy bands become discrete quantum energy states. Whereas in bulk the wave function is distributed across the entire crystal as Bloch waves, $u_{\mathbf{k}}(\mathbf{r})e^{i\mathbf{k}\cdot\mathbf{r}}$, in nanocrystals the wave function is confined by the surfaces. The size of the nanostructure directly impacts the energy states, analogous to the elementary particle-in-a-box problem. Consider, for example, a [110] Ge nanowire. When the wire diameter is sufficiently small the crystal's translational symmetry is only meaningful in the [110] direction and the bulk Ge states are projected along the $\mathbf{k}$=[110] direction in k space. This projection transforms Ge from an indirect to direct band-gap material.[43] The confinement is predicted to distort the shape of the energy dispersion for wires with diameters as large as 2 nm. The energy bands of nanowires with diameter greater than 2 nm are found to undergo a rigid shift, even for wires as large as 5 nm.[43]

Fundamentally, there are two effects that differentiate the behavior of defects in nanostructures from bulk: quantum confinement and free surfaces. Dalpian[44] claims that the confinement of the defect's wave function results in the so-called *self-purification* effect that increases the defect's ΔE_f^{η}. In the case of dopant species, this increase hinders the incorporation of dopant atoms into the nanostructures. This is a controversial subject and worthwhile investigating.[45–47] In the present calculations evidence of self-purification will be sought.

The free surfaces allow the nanostructure to expand or contract to reduce the strain energy surrounding the defect. From an energetics perspective the self-purification effect and the free surfaces compete with one another. The self-purification increases the energy and the free surfaces decrease the energy. From a kinetics perspective they comple-

ment one another because it is likely that the surfaces will getter impurities out of the nanostructure. In the case of Si nanocrystals it is observed that the relative energy to introduce vacancies decreases as the nanocrystal's size decreases. This indicates that energetically the free surfaces dominate the self-purification effect.[48] As the vacancy is moved toward the surface the energy further decreases and when the vacancy is within 0.6 Å of the surface it becomes unstable and is spontaneously moved to the surface of the crystal.[48,49]

In this paper the structure and energies of vacancies in Ge nanocrystals are examined as a function of the nanocrystal's size and the position of the vacancy in the crystal. Because the energies, ΔE_f^η, depend on the size of the crystal and the position within the crystal, the concentrations and diffusivities, from Eqs. (2) and (3), also depend on the size and position. Self-diffusion within nanostructures is not a simple matter that can be easily described by a single coefficient. The work here is a first step toward building a comprehensive model.

Following this introduction, in Sec. II, the methods used will be presented, including a discussion of the computational approach and the details of the nanocrystals' morphology. The results from these calculations will be presented and discussed in Sec. III. A concluding summary will be presented in Sec. IV.

II. METHODS

A. Computational approach

The calculations are performed within the framework of the density-functional theory[50] (DFT), using the local-density approximation[51] (LDA) for the exchange-correlation functional, as it is implemented in the SIESTA computational package.[52] The electrons in the core atomic region are substituted by norm-conserving pseudopotentials of the Troullier-Martins type,[53] and the valence charge is represented by a set of atom-centered basis functions. In SIESTA these functions correspond to numerical atomic orbitals of strictly finite range, a particular choice that is specially suited to treat isolated systems.

All calculations are carried out using a double-ζ plus polarization orbitals basis set. The cut-off radii of the basis functions are optimized for bulk germanium in the diamond structure, following the method proposed in Ref. 54, where a fictitious external pressure of 0.2 GPa is employed on the free atom. This basis size and radius lengths are proven to give a good balance between the computational accuracy and cost. A theoretical lattice parameter of $a_0=5.64$ Å and a bulk modulus of $B_0=80.0$ GPa are obtained from the fitting to the Murnaghan equation of state.[55] Both values are in good agreement with the structural and elastic properties from experiments[56] ($\tilde{a}_0=5.66$ Å and $\tilde{B}_0=75.8$ GPa), given the fact that the LDA tends to underestimate lattice constants by a 1–3 % but also to overestimate bulk moduli with errors ranging from 5% up to 20%.[57]

The theoretical method employs periodic boundary conditions. The nanocrystals are placed inside the supercell surrounded by a buffer of empty space. The size of the atomic clusters ranges from 44 to 244 Ge atoms and the vacuum region is chosen to be large enough as to avoid any interaction between their periodic replicas. A kinetic-energy cutoff of 250 Rydberg is chosen for the real-space integrations involving the Hartree and the exchange-correlation contributions to the self-consistent potential. In this respect, a stringent criterion is employed in the convergence of the density matrix and total energy. All atomic coordinates are then relaxed according to a conjugate-gradient minimization algorithm, until the maximum residual forces are below 0.02 eV/Å.

B. Nanocrystal morphology

The nanocrystal geometries used in these studies are hydrogen-passivated, bond-centered crystals. Experimental nanostructures frequently have amorphous, glassy, or polymeric coatings that result from the method of crystal growth. It is possible to treat the surfaces to reduce or remove these, although it is uncommon experimentally to work with bare surfaces. The nanocrystals investigated here have their surfaces passivated with an extremely "soft" H pseudopotential. Surface passivation removes surface states and allows the competition between the self-purification effect and the free surfaces to be studied without considering the complicated surface chemistry.

Surface Ge atoms are identified and the dangling bonds of the Ge atoms are capped with H. Any Ge atom that is found to have three dangling bonds is replaced by a single H atom. The resulting nanocrystals are shown in Fig. 1. The surface morphologies are examined and crystals that are highly faceted are excluded. Only nanocrystals with near spherical geometry are studied.

III. RESULTS AND DISCUSSION

A. Atomic structure and defect states

The local atomic structure at the vacancy site is directly related to the electronic states introduced to the gap from the broken bonds. The atomic structure of the vacancy in the 1.02 and 2.20 nm nanocrystals is given in Table II, using as reference the ABCD indices shown in Fig. 2. The associated electronic states are diagrammed in Fig. 3. The left column of Fig. 3 shows the states for a nanocrystal with no vacancy. The band gap for the 1.02 nm crystal is 3.13 eV and the gap for the 2.20 nm crystal is 2.0 eV.

An undistorted vacancy has T_d symmetry. There are three degenerate states in the gap, belonging to the t_2 representation, associated with this structure. These are shown in the middle column of Fig. 3. There are two electrons localized at the defect so the states are partially occupied. It is the partial occupancy of the degenerate energy levels that allows the defect to undergo a spontaneous symmetry breaking that reduces the degeneracy and lowers the electronic energy. In bulk crystals the Jahn-Teller distortion produces a D_{2d}-symmetrized structure with the fully occupied state belonging to the b_2 representation and the doubly degenerate, empty state having the e representation.[48,58,59]

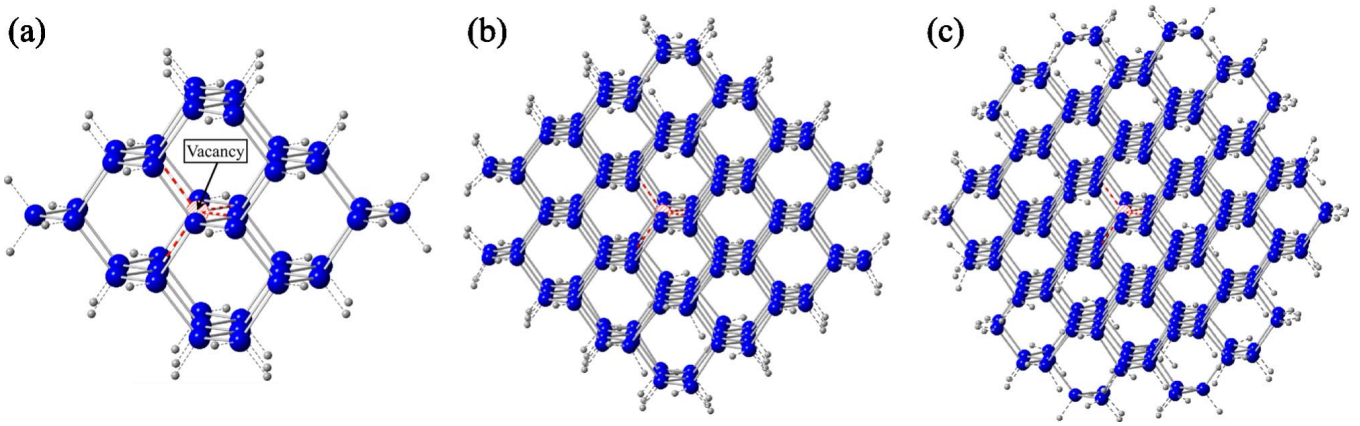

FIG. 1. (Color online) Ge nanocrystal morphology for (a) $Ge_{44}H_{42}$, (b) $Ge_{130}H_{98}$, and (c) $Ge_{244}H_{158}$. The corresponding sizes are 1.02, 1.70, and 2.20 nm, respectively. A central vacancy is depicted as a hatched atom surrounded by four missing bonds (broken lines), all in red. Ge atoms are colored in blue (dark gray); saturating H atoms are in light gray.

Here, as in the case of a vacancy in a Si nanocrystal,[48] the symmetry of the structure approaches D_{2d} but due to the surfaces there is additional distortion. In the case of the 1.02 nm crystal, the symmetry of the vacancy structure is C_s. For the 2.20 nm crystal the symmetry is essentially D_{2d} but a minuscule 0.01 nm distortion of the bonds lowers the symmetry, i.e., if $\overline{AC}=\overline{AD}=\overline{BC}=\overline{BD}$ then the symmetry would be D_{2d}. From Table II it is determined that the Jahn-Teller distortion in the 1.02 nm crystal is approximately 10% larger than that in the 2.20 nm crystal and as a result the defect states undergo a larger energy split, over 2.7 eV, which almost pushes the states out of the gap. In the 2.20 nm crystal the splitting is much smaller, around 0.75 eV.

B. Crystal size

The energy of the fully optimized vacancy structures in the different sized nanocrystals is calculated. Subtracting this energy from the energy of the perfect nanocrystals yields the energy of formation for a vacancy plus the chemical potential for Ge, i.e., the energy to remove a Ge atom from the system. The chemical potential is variable and depends on the local chemical environment. By assuming that all the nanocrystals are located in the same environment and have the same chemical potential it is possible to compare the relative energy of formation for vacancies in different sized nanocrystals. It is known that as a nanocrystal's diameter approaches infinity the energy of formation approaches that found in bulk Ge. Using this energy limit the calculated energy of formation versus crystal diameter is plotted in Fig. 4(a). It is assumed that the size dependence goes as

$$E(D) = \frac{\alpha}{D^{\beta}} + \gamma, \tag{4}$$

where α, β, and γ are fitting coefficients. In the limit that the diameter, D, goes to infinity, the energy equals γ. The coefficients are determined to be $\alpha=-1.1395$ eV and $\beta=6.2574$. The energy zero is shifted so that $\gamma=2.0$ eV, which is taken from the energies reported in Table I. The quality of this fit appears good. It is observed that the energy of formation is near the bulk value for crystals as small as 2.0 nm. This is surprising because quantum confinement continues to

TABLE II. The local bond lengths (in Å) at a vacancy site in crystals with diameters 1.02 and 2.20 nm. The segment labels reference the tetrahedral structure in Fig. 2. Using the DFT-LDA the theoretical bond length in bulk Ge is 2.44 Å, which corresponds to segment lengths of 3.99 Å before atomic relaxation.

Segment	$D=1.02$ nm	$D=2.20$ nm
$\overline{AB}$	2.55	2.90
$\overline{AC}$	3.57	3.47
$\overline{AD}$	3.57	3.47
$\overline{BC}$	3.79	3.46
$\overline{BD}$	3.79	3.46
$\overline{CD}$	2.50	2.90

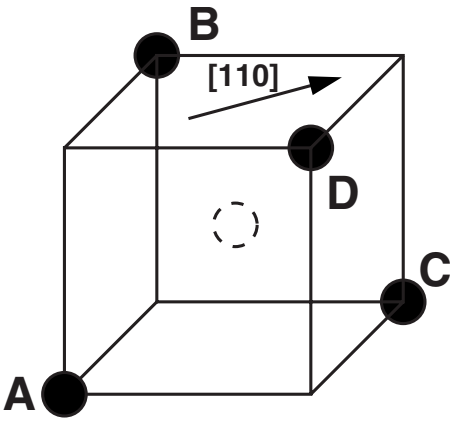

FIG. 2. The reference geometry of the atomic structure at the vacancy site. The dashed circle is the vacancy and the solid circles are the nearest-neighbor Ge atoms that form a tetrahedron. The tetrahedron, without atomic motion has T_d symmetry. The calculated bond lengths for various sized nanocrystals are shown in Table II.

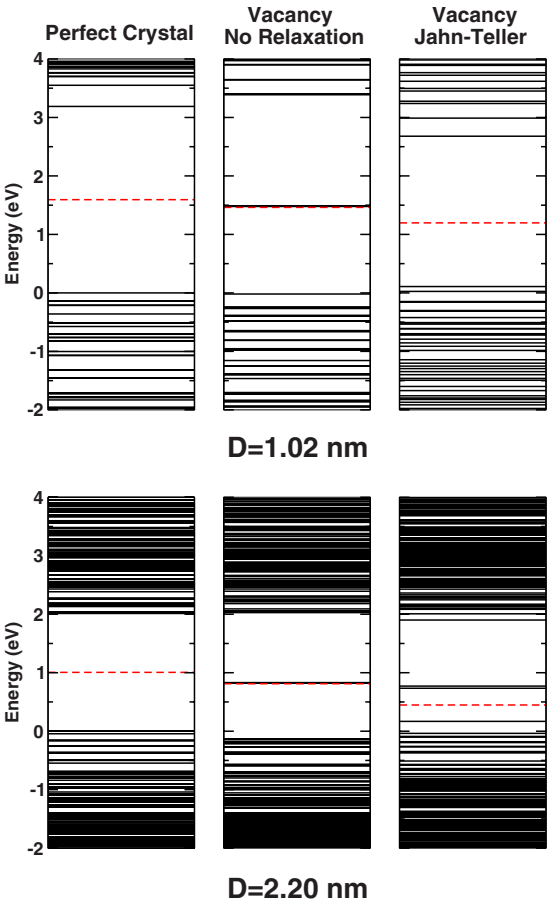

FIG. 3. (Color online) The top frame shows the energy levels for a crystal with 1.02 nm diameter and the bottom frame shows a 2.20 nm crystal. The red dashed line is the Fermi energy. The band alignment between the diagrams is arbitrary. The crystals in the left column are perfect and contain no vacancy. The crystals in the center column have vacancies, but the structure has not been allowed to relax. The states at the Fermi level are threefold degenerate. The right column shows the states after the Jahn-Teller distortion is completed, which allows the atomic structure to break the symmetry and lift the degeneracy of the gap state.

strongly influence the band gap for crystals with a similar size, as shown in Fig. 4(b).

C. Distance from crystal center

To determine the influence of a vacancy's position on its energy a 2.20 nm crystal ($Ge_{244}H_{158}$) is examined with a vacancy at various locations within it. The calculated energies are shown in Fig. 5. The configuration where the vacancy is adjacent to the center of the crystal [Fig. 1(c)] is defined as the zero. Near the center of the crystal there is little change in the energy, but once the vacancy is within 0.7 nm of the surface it begins to drop substantially. The last stable vacancy site is 0.3 nm from the surface. The energy of a vacancy at this site is a full 1.2 eV less than a vacancy near the center. From the results in Sec. III B it is known that the energy of formation in the center of the 2.20 nm crystal is almost that observed in bulk or slightly smaller. Using the

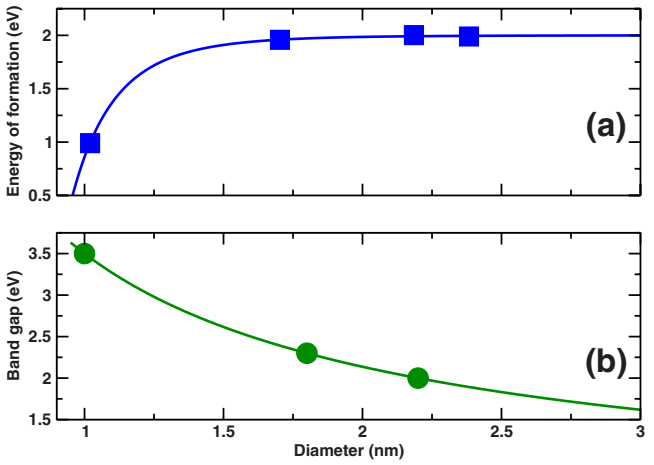

FIG. 4. (Color online) The relative energy of formation for a vacancy in different sized nanocrystals is plotted in frame (a). In frame (b) band gap is plotted versus the crystal size. The solid lines show Eq. (4) with the coefficients fitted to the data.

energies in Table I it is deduced that the energy of formation for the vacancies near the surface can be no larger than 0.5–1.4 eV.

IV. CONCLUSION

A vacancy in a Ge nanocrystal undergoes a Jahn-Teller distortion. The T_d-symmetrized broken bonds located at the vacancy introduce a set of threefold degenerate, partially occupied, states in the gap. When these dangling bonds reconstruct the defect symmetry is lowered. This reduces the degeneracy of the defect states by splitting them into a lower-energy, fully occupied state and two higher-energy, degenerate empty states. In a bulk crystal it is known that the symmetry of the vacancy site is D_{2d},[58] but in the nanocrystals the surfaces introduce additional distortion. For the smallest crystal the surface influence is great; the defect symmetry is C_s and the energy splitting is approximately 2.7 eV. This results in a dramatic reduction in the energy of formation. In

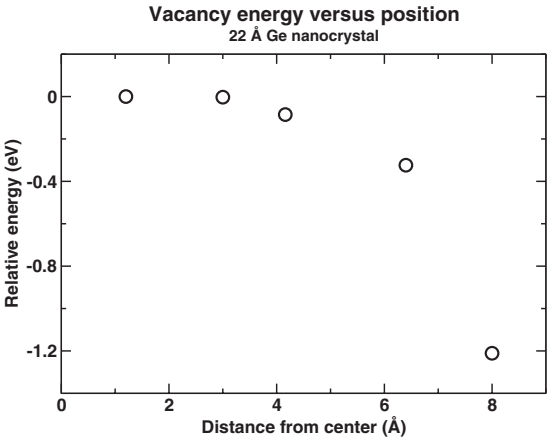

FIG. 5. The relative energy of a vacancy in a 2.20 nm Ge nanocrystal ($Ge_{244}H_{158}$). The zero of the energy scale is defined to be the innermost atomic site.

the 2.20 nm crystal the defect almost has the D_{2d} symmetry that is found in bulk. The energy splitting is also smaller than that in the 1.02 nm crystal, only around 0.75 eV; therefore, the energy reduction due to the bond reconstruction is lower and the energy of formation is larger in the 2.20 nm crystal. This is consistent with the calculated prediction that the energy of formation will approach the bulk value for nanocrystals larger than 2.0 nm.

The band gap of the crystal continues to change greatly even when the diameter is as large as 2 nm. It is deduced that although quantum confinement continues to impact the energy levels in the crystal, the primary influence on the vacancy is the surface's ability to enhance the internal structural relaxation. It is concluded that in this example the quantum self-purification effect plays a small role if any. A similar observation has been made for vacancies in Si.[48] It is hypothesized that this is due to the defect's wave function being highly localized at the reconstruction bonds.

Finally, it is determined that vacancies placed within 0.7 nm of the surface are spontaneously removed. Surprisingly vacancies in the interior of the crystal are stable and do not appear to be drawn toward the exterior. An additional consequence is that if a surface were to act as a vacancy source, the vacancies produced from the surface are unlikely to penetrate deeply into the nanocrystal. The system studied here has H-passivated surfaces, which allows for large relaxations. Experimental crystals that have surface reconstructions or polymer coatings will have more rigidity and the influence of the surfaces will be further muted inside the crystal.

The picture that emerges from this work is that moderate sized crystals will have an interior where vacancies behave bulklike and a thin exterior surface region where the surface effects will dominate. Assuming that the properties of the self-interstitial defect are not strongly modified by the surfaces, then the evidence in this paper predicts that the self-diffusion in the interior of Ge nanocrystals will not be substantially different from that observed in bulk. However, recent experiments indicate that Ge surfaces are not sinks for interstitial atoms, but instead reflect the interstitial Ge back into the crystal.[31] If this observation holds within the nanoregime then it is possible that the large surface to volume ratio in nanostructures will magnify the impact of the interstitial-assisted diffusion.

ACKNOWLEDGMENT

The authors gratefully acknowledge support from the National Science Foundation under Grant No. DMR-0755231.

*Present address: Institut de Ciència de Materials de Barcelona, ICMAB-CSIC, Campus UAB, 08193 Bellaterra, Spain.
†sbeckman@iastate.edu

[1] P. Y. Yu and M. Cardona, *Fundamentals of Semiconductors*, 3rd ed. (Springer, New York, 2001).
[2] C. O. Chui, K. Gopalakrishnan, P. B. Griffin, J. D. Plummer, and K. C. Saraswat, Appl. Phys. Lett. **83**, 3275 (2003).
[3] M. L. Lee, C. W. Leitz, Z. Cheng, A. J. Pitera, T. Langdo, M. T. Currie, G. Taraschi, E. A. Fitzgerald, and D. A. Antoniadis, Appl. Phys. Lett. **79**, 3344 (2001).
[4] H. L. Shang *et al.*, Tech. Dig. - Int. Electron Devices Meet. 2002, 441.
[5] C. O. Chui, S. Ramanathan, B. B. Triplett, P. C. McIntyre, and K. C. Saraswat, IEEE Electron Device Lett. **23**, 473 (2002).
[6] M. L. Lee, E. A. Fitzgerald, M. T. Bulsara, M. T. Currie, and A. Lochtefeld, J. Appl. Phys. **97**, 011101 (2005).
[7] H. Shang, J. O. Chu, X. Wang, P. M. Mooney, K. Lee, J. Ott, K. Rim, K. Chan, K. Guarini, and M. Ieong, Dig. Tech. Pap. - Symp. VLSI Technol. 2004, 204.
[8] H. Shang, M. M. Frank, E. P. Gusev, J. O. Chu, S. W. Bedell, K. W. Guarini, and M. Ieong, IBM J. Res. Dev. **50**, 377 (2006).
[9] Z. Y. Cheng, J. W. Jung, M. L. Lee, A. J. Pitera, J. L. Hoyt, D. A. Antoniadis, and E. A. Fitzgerald, Semicond. Sci. Technol. **19**, L48 (2004).
[10] H. J. Queisser and E. E. Haller, Science **281**, 945 (1998).
[11] H. Bracht, MRS Bull. **25**, 22 (2000).
[12] P. Ganster, G. Treglia, and A. Saul, Phys. Rev. B **79**, 115205 (2009).
[13] Y. Shimizu, M. Uematsu, and K. M. Itoh, Phys. Rev. Lett. **98**, 095901 (2007), and references therein.
[14] J. Zhu, T. Diaz dela Rubia, L. H. Yang, C. Mailhiot, and G. H. Gilmer, Phys. Rev. B **54**, 4741 (1996).
[15] B. Sahli and W. Fichtner, Phys. Rev. B **72**, 245210 (2005).
[16] S. A. Centoni, B. Sadigh, G. H. Gilmer, T. J. Lenosky, T. D. de la Rubia, and C. B. Musgrave, Phys. Rev. B **72**, 195206 (2005).
[17] W. K. Leung, R. J. Needs, G. Rajagopal, S. Itoh, and S. Ihara, Phys. Rev. Lett. **83**, 2351 (1999).
[18] A. Antonelli, E. Kaxiras, and D. J. Chadi, Phys. Rev. Lett. **81**, 2088 (1998).
[19] C. Z. Wang, C. T. Chan, and K. M. Ho, Phys. Rev. Lett. **66**, 189 (1991).
[20] A. F. Wright, Phys. Rev. B **74**, 165116 (2006).
[21] A. Fazzio, A. Janotti, A. J. R. da Silva, and R. Mota, Phys. Rev. B **61**, R2401 (2000).
[22] A. J. R. da Silva, A. Janotti, A. Fazzio, R. J. Baierle, and R. Mota, Phys. Rev. B **62**, 9903 (2000).
[23] B. P. Uberuaga, G. Henkelman, H. Jonsson, S. T. Dunham, W. Windl, and R. Stumpf, Phys. Status Solidi B **233**, 24 (2002).
[24] A. Carvalho, R. Jones, C. Janke, J. P. Goss, P. R. Briddon, J. Coutinho, and S. Öberg, Phys. Rev. Lett. **99**, 175502 (2007).
[25] C. J. Hwang and L. A. K. Watt, Phys. Rev. **171**, 958 (1968).
[26] A. Chroneos, R. W. Grimes, B. P. Uberuaga, and H. Bracht, Phys. Rev. B **77**, 235208 (2008), and references therein.
[27] H. Pinto, J. Coutinho, V. Torres, S. berg, and P. Briddon, Mater. Sci. Semicond. Process. **9**, 498 (2006).
[28] M. D. Moreira, R. H. Miwa, and P. Venezuela, Phys. Rev. B **70**, 115215 (2004).
[29] J. Vanhellemont, P. Śpiewak, and K. Sueoka, J. Appl. Phys. **101**, 036103 (2007).
[30] H. H. Silvestri, H. Bracht, J. L. Hansen, A. N. Larsen, and E. E.

Haller, Semicond. Sci. Technol. **21**, 758 (2006).
[31] H. Bracht, S. Schneider, J. N. Klug, C. Y. Liao, J. L. Hansen, E. E. Haller, A. N. Larsen, D. Bougeard, M. Posselt, and C. Wündisch, Phys. Rev. Lett. **103**, 255501 (2009).
[32] M. Werner, H. Mehrer, and H. D. Hochheimer, Phys. Rev. B **32**, 3930 (1985).
[33] H. Bracht, H. H. Silvestri, I. D. Sharp, and E. E. Haller, Phys. Rev. B **75**, 035211 (2007).
[34] H. Bracht, N. A. Stolwijk, and H. Mehrer, Phys. Rev. B **43**, 14465 (1991).
[35] S. Brotzmann, H. Bracht, J. L. Hansen, A. N. Larsen, E. Simoen, E. E. Haller, J. S. Christensen, and P. Werner, Phys. Rev. B **77**, 235207 (2008).
[36] A. Chroneos, H. Bracht, R. W. Grimes, and B. P. Uberuaga, Appl. Phys. Lett. **92**, 172103 (2008).
[37] S. Das, R. K. Singha, K. Das, A. Dhar, and S. K. Ray, J. Nanosci. Nanotechnol. **9**, 5484 (2009).
[38] X. Ma and C. Wang, Appl. Phys. B: Lasers Opt. **92**, 589 (2008).
[39] S. Sato, H. Morisaki, and M. Iwase, Appl. Phys. Lett. **66**, 3176 (1995).
[40] L. N. Zhang, J. He, J. Zhang, F. Liu, Y. Fu, Y. Song, and X. Zhang, IEEE Trans. Electron Devices **55**, 2907 (2008).
[41] Y. Jiang *et al.*, IEEE Electron Device Lett. **29**, 595 (2008).
[42] T. Markussen, R. Rurali, A. P. Jauho, and M. Brandbyge, Phys. Rev. Lett. **99**, 076803 (2007).
[43] S. P. Beckman, J. X. Han, and J. R. Chelikowsky, Phys. Rev. B **74**, 165314 (2006).
[44] G. M. Dalpian and J. R. Chelikowsky, Phys. Rev. Lett. **96**, 226802 (2006).
[45] M. H. Du, S. C. Erwin, A. L. Efros, and D. J. Norris, Phys. Rev. Lett. **100**, 179702 (2008).
[46] G. M. Dalpian and J. R. Chelikowsky, Phys. Rev. Lett. **100**, 179703 (2008).
[47] J. B. Li, S. H. Wei, S. S. Li, and J. B. Xia, Phys. Rev. B **77**, 113304 (2008).
[48] S. P. Beckman and J. R. Chelikowsky, Physica B **401**, 537 (2007).
[49] S. P. Beckman and J. R. Chelikowsky (unpublished).
[50] W. Kohn and L. J. Sham, Phys. Rev. **140**, A1133 (1965).
[51] D. M. Ceperley and B. J. Alder, Phys. Rev. Lett. **45**, 566 (1980).
[52] J. M. Soler, E. Artacho, J. D. Gale, A. García, J. Junquera, P. Ordejón, and D. Sánchez-Portal, J. Phys.: Condens. Matter **14**, 2745 (2002).
[53] N. Troullier and J. L. Martins, Phys. Rev. B **43**, 1993 (1991).
[54] E. Anglada, J. M. Soler, J. Junquera, and E. Artacho, Phys. Rev. B **66**, 205101 (2002).
[55] F. D. Murnaghan, Proc. Natl. Acad. Sci. U.S.A. **30**, 244 (1944).
[56] O. Madelung, U. Rössler, and M. Schulz, *Group IV Elements, IV-IV and III-V Compounds Part a*, Landolt-Börnstein Database Vol. 41A1a (Springer-Verlag, Berlin, 2001).
[57] D. R. Hamann, Phys. Rev. Lett. **76**, 660 (1996).
[58] G. D. Watkins, *Deep Centers in Semiconductors* (Gordon and Breach Science, New York, 1986), Chap. 3, p. 147.
[59] S. Ögüt and J. R. Chelikowsky, Phys. Rev. B **64**, 245206 (2001).